

# Working principle analysis and control algorithm for bidirectional DC/DC converter

B. Y. Li<sup>a,\*</sup>, C. Xu<sup>a</sup>, C. Li<sup>b</sup>, Z. Guan<sup>a</sup>

<sup>a</sup>School of Information Science and Engineering, Dalian Polytechnic University, Dalian, 116034, China;

<sup>b</sup>School of Electrical Engineering and Telecommunications, The University of New South Wales, Sydney, NSW 2052, Australia

## Abstract

A bidirectional DC/DC converter is an important part of the DC micro grid system, playing a key role in the stable operation of the system and the coordinated distribution of power. To solve the problem of unstable busbar voltage when the energy transforms bidirectionally in the DC micro grid system, a control algorithm based on closed-loop proportion integral derivative was proposed in this study. The hardware circuit of the bidirectional DC/DC converter was designed in the DC micro grid energy storage system, and the characteristics of converter efficiency in charging mode and constant voltage output were studied by small-signal modeling of the bidirectional DC/DC converter in charging and discharging systems. Experimental data were used to prove the correctness of the theoretical analysis. The results demonstrate that the current-controlled precision changes steadily in the charging mode when the output voltage is constant and the charging current is adjustable in ranges between 1 A and 2 A. When the charging current is 2 A and the output voltage ranges from 24 V to 36 V, the change rate of the charging current undergoes stable changes. In the discharge mode, when the output voltage is stable, the converter conversion rate changes steadily. When the output voltage changes in the range between 32 V and 38 V, the bidirectional DC/DC circuit automatically switches over the work patterns and maintains the stability of the output voltage. This study achieves bidirectional transmission of energy by rational hardware design of a bidirectional DC/DC converter and improves the reliability of the DC micro grid energy storage system. The proposed method provides a good prospect of a control scheme for the bidirectional DC/DC converter to optimize practical engineering design.

**Keywords:** DC micro grid system; Bidirectional DC/DC converter; STM32F103RBT6 microcontroller; Closed-loop PID control

## 1. Introduction

The bidirectional DC/DC converter comes from the common unidirectional DC/DC converter and can achieve energy flow in two directions. Electronic equipment in markets cannot work without a stable power supply system. With the development of technology, the number of types of electronic products is steadily increasing. The stability of the power supply system is key to guaranteeing good working conditions in electronic production. Moreover, the performance of the power supply directly influences the safety and stability of electronic equipment.

At present, numerous uses of renewable energy sources, such as wind and solar energy, have received considerable attention in the context of a micro grid system. A micro grid system develops rapidly and is an independent and controllable power supply system that consists of an energy storage system, micro power supply, energy conversion device, and

load. Specifically, the DC micro grid system operates without problems in frequency stability, reactive power regulation, and AC loss and can connect with new energy, electric vehicles, and other equipment. A DC micro grid can be used for data centers, residential areas, and other public places [1]. In the DC micro grid system, the energy storage system is crucial, and the bidirectional DC/DC converter is its control core. A reasonable design of a DC micro grid system can optimize the operation of micro power supply. In the study of micro grid voltage stability, the key aspects are the hardware circuit and the controlling method in the bidirectional DC/DC converter, which is related to the flow of the energy storage unit. The converters control the energy flow direction of the bidirectional DC/DC converter as well as the energy storage unit to maintain the stability of the DC micro grid voltage, which can satisfy the grid operation conditions [2, 3].

In a traditional DC converter, the transmission of current is unidirectional, because the reverse breaks down in switching devices, such as the metal-oxide-semiconductor field-effect transistor (MOSFET) and the insulated gate bipolar transistor (IGBT). Moreover, the main circuit has a freewheeling

\*Corresponding author

Email address: liby@dlpu.edu.cn (B. Y. Li)

diode and works in the forward conduction state, in which the problem of the current being unable to reverse breakdown is shown. A specific power supply system often needs energy that works in a bidirectional direction using an anti-parallel method between the common AC converters that fulfills the purpose of energy reverse circulation to a certain extent. However, only one converter is operational each time, which results in a waste of resources.

Based on the above analysis, this study adopts the bidirectional DC/DC converter to increase the conversion efficiency by reducing the necessary elements to replace the DC converter in bidirectional directions, which works in the transmission channel between the AC busbar voltage and the energy shortage unit, to achieve bidirectional flow of energy. Bidirectional DC/DC converters have considerable contributions to make in terms of saving energy and protecting the environment; therefore, studying bidirectional DC/DC converters is meaningful for the future.

## 2. State of the art

Numerous studies have been conducted on bidirectional DC/DC converters. The bidirectional DC/DC converter outputs DC voltage by filtering the time ratio of opening and closing of the switch transistor. With the technical progress of integrated circuits, bidirectional DC/DC converters are moving toward integrated development and miniaturization [4]. The bidirectional DC/DC converter mainly uses pulse width modulation (PWM) and combines it with power electronic technology. DC/DC switching power is a highly efficient power supply type and it has become a focus of attention in the development of DC power supply. As various high and new technologies develop, so does DC/DC converter technology [5].

In 2000, Xu M. David [6] proposed a high-efficiency ZCT-PWM full bridge DC/DC converter in Zhejiang University using the method of parallel resonant network in an output rectifier circuit. The efficiency of voltage conversion reached 96% using the 5 kW–100 kHz IGBT-SMPS model and resulted in poor overall stability. Ramya K.C and Jegathesan V [7] analyzed the topology of the bidirectional DC/DC converter and proposed a proportional integral (PI) and a proportion integral derivative (PID) control method by using the open-loop control algorithm. However, the proposed system was unable to effectively control the error signals and could not maintain stability at constant pressure and current. Jabbour N et al. [8] suggested the use of a lift motor driven by a super capacitor energy storage, which controlled the DC/DC converter in the best way through online adjustment of the DC link voltage PI control technology. However, during operation, the storage capacity in the power output side was difficult to control and the structure of the system was complex. Borocci G et al. [9] analyzed the bidirectional DC/DC converter and posted a buck-boost topology, which could overcome the problem of unsuitability of the bidirectional DC/DC converter for the capacity of the electric vehicle to address situations where the input and output power storage were in opposite polarity.

China started late in the study of the DC/DC converter. Chen Qingquan [10], a Chinese academic who is known as the father of the Asian electric vehicle, proposed applying a bidirectional DC/DC converter on the electric vehicle to improve its power, but the use of IGBT was costly and it was difficult to control. Jiang Dan and Liu Fuxin [11] proposed a three-port converter with integrated buck-boost and coupled inductor technology, which used two reverse coupling inductances to further improve the performance of the converter and control the efficiency of constant output voltage and constant current output effectively, by making a structure similar to the inductor interleaved bridge arm. The authors realized that the current could be expanded and ripple wave was inhabited. In 2014, a new type of dual active bidirectional DC/DC converter was proposed by Cai Yingying et al. [12], which applied the LCC (Line-commutated Converter) resonant tank to the traditional isolation-based bidirectional full bridge (dual active bridge, DAB) DC/DC converter, and analyzed a DC/DC converter that could make bidirectional power transmission. However, the system must be part of a resonant capacitor at the end of the transformer to form LCC resonant topology, its structure was complex, and the topological structure could only be applied in high-power and high-frequency applications. Lin Peng [13] in May 2017 designed a computer-controlled bidirectional DC/DC converter, which collected the battery in the charge or discharge state of the current and the voltage signal to the AD converter. The microcontroller applied the PID algorithm to calculate the amount of control with PWM pulse to control the turn-on time of the bidirectional DC/DC converter, to complete the battery constant current charging or constant voltage discharge, and to achieve the energy bidirectional flow. However, STC12C5A16S2 was selected as the controller and used the PID algorithm. The PID control algorithm cannot determine use of the open-loop control or closed-loop control so that the system could achieve bidirectional DC/DC conversion, and could not test output stability at constant voltage and constant current. Wei Xing and Dai Desong [14] proposed the bidirectional closed-loop PID control algorithm to control the bidirectional DC/DC converter, but the robustness of the controller was weak in this controlling method, which resulted in a contradiction between the overshoot and the transition time. Therefore, the efficiency of the output voltage was not relatively stable. Zhao Langtao et al. [15] analyzed the control strategy of the bidirectional DC/DC converter and proposed the use of the STC89C51 microcontroller as the core to control the converter. However, the controller could not achieve multiple AD current acquisitions and thus the model was not accurate enough in the design.

Based on the above analysis, a closed-loop PID control algorithm is proposed to realize the DC step-down to lithium battery in the bidirectional DC/DC converter control system and achieve the boost reservedly in the lithium battery to the load power supply, which has good stability and accuracy. The bidirectional DC/DC converter can greatly reduce the weight and volume of the power supply equipment and has high application value and broad development prospects.

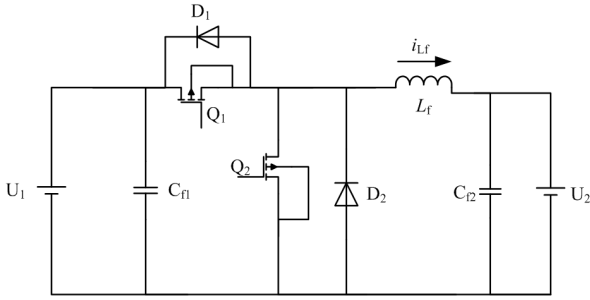


Figure 1: Topological structure of the bidirectional buck-boost DC/DC converter

The remainder of this study is organized as follows. Section 3 presents a topology analysis of the DC/DC converter circuit, hardware design, implementation of the closed-loop PID control algorithm and the design of the software diagram. Section 4 mainly describes the experiment measurement and analysis of the result. The last section summarizes the conclusions.

### 3. Methodology

#### 3.1. Topology principle of the bidirectional DC/DC converter

Half bidirectional bridge topology combines the unidirectional buck and boost converters. The basic topology of the bidirectional DC/DC converter is shown in Fig. 1. For the high-voltage side of the power supply, the power input voltage, diode, switch tube, and capacitor are represented by  $U_1$ ,  $D_1$ ,  $Q_1$  and  $C_{f1}$ , respectively. For the low-voltage side of the power supply, the power output voltage, switch tube, diode, and capacitor are represented by  $U_2$ ,  $Q_2$ ,  $D_2$  and  $C_{f2}$ , respectively. The diode is added in the position of the switch tube in the basic one-way buck converter, and the switch tube is placed in the original position of the diode, which is composed of a buck-boost type of bidirectional DC/DC converter circuit to control the state of the two switch tubes and further control the direction of the current and the values of the voltage and current [16].

When  $Q_1$  is switched on and  $Q_2$  is switched off, the forward current flows through  $Q_1$  and  $D_2$ . At this point, the energy is transmitted through the high-voltage side of the DC power supply to the low-voltage side of the lithium battery, and the depressurization process is completed. Hence, the buck-boost bidirectional DC/DC converter is equivalent to the unidirectional buck converter circuit at this point. The energy in the system is transmitted to the low-voltage side of the lithium battery through the high-voltage side of the DC power supply. When  $Q_2$  is switched on,  $Q_1$  is switched off,  $Q_2$  and  $D_1$  are in parallel, which constitutes a unidirectional boost circuit, and the value of voltage rises; the energy is then boosted from the low-voltage side of the lithium battery. This combined design not only achieves bidirectional flow of energy but also retains the equivalent circuit of basic buck and boost topologies [17].

To prevent the power circuit from working in a switch-off state that may damage the equipment, the two switch tubes  $Q_1$  and  $Q_2$  are restrained from being connected simultaneously. The proper dead time  $T_d$  should be set between the driving signals, i.e.,  $Q_2$  can be switched on after experiencing delay time  $T_d$  and  $Q_1$  switches off. Moreover, after switching off  $Q_2$  and experiencing delay time  $T_d$ ,  $Q_1$  switches on to prevent the short circuit from damaging the system. The main reason is the energy storage inductance in the main circuit. However, to achieve switch-on of the switch in zero voltage, the Schottky diode is needed at both ends of the switch tube, which is used for the current freewheeling after the switch tube is switched off.

When the circuit works in buck mode, the energy is transmitted forward, and the current in the inductor flows from the high-voltage side to the low-voltage side. When the circuit operates in boost mode, the current in the inductor flows from the low-voltage side to the high-voltage side. The polarity of the voltage  $U_1$  and  $U_2$  is the same at both ends of the circuit, because the circuit works in forward or reverse direction. Hence, in this situation, this type of bidirectional DC/DC converter is called the current bidirectional DC/DC converter [18].

The main work of bidirectional DC/DC converter is to regulate the output voltage by regulating the duty cycle by PWM through MOSFET according to a certain frequency and duty ratio. In this topology, the independent PWM control mode is adopted in the DC micro grid system (the independent PWM control mode is utilized in the time-sharing control in buck and boost modes). When the lithium battery works in a charging state, the buck circuit continues to work. At this point,  $Q_1$  is switched on by controlling PWM, and  $Q_2$  is the switch-off state. When the battery discharges, the boost circuit continues to operate and, at this point,  $Q_2$  is switched on by controlling PWM. Therefore, the system works in the independent PWM control mode, and buck and boost modes cannot cause interference [19].

In the bidirectional DC/DC converter, iron-silicon aluminum is used as the magnetic core, which has the advantages of low magnetic core loss and temperature stability. Equation (1) demonstrates that the value of inductive energy storage is calculated by the system. In Equation (1), the inductor  $L$  is  $200 \mu\text{H}$ ;  $U_i$  is the input voltage of the converter;  $D$  is the duty ratio of the PWM signal, which ranges from 0 to 1;  $I_{\max}$  is the maximum current of inductance  $L$ ; and  $f_s$  is the frequency of alternating current (AC) [20].

$$L \geq \max \left[ \frac{U_i D (1 - D)}{f_s I_{\max}} \right] = \frac{35 \cdot 0.5 \cdot 0.5}{50k \cdot 2} = 87.5 \mu\text{H} \quad (1)$$

#### 3.2. Working principle of the buck circuit

According to the continuous current of the inductor, the buck structure consists of three states, namely, continuous, discontinuous, and critical. When the current in the output energy storage inductor is always greater than zero, the current is continuous. If the inductor current is zero at the

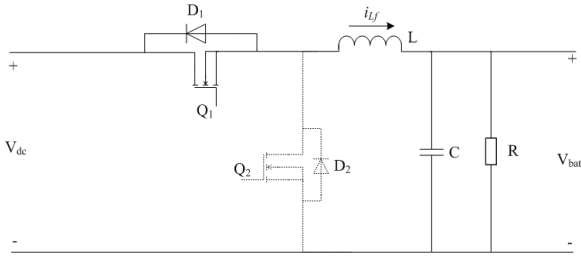


Figure 2: Equivalent circuit state of buck mode 1

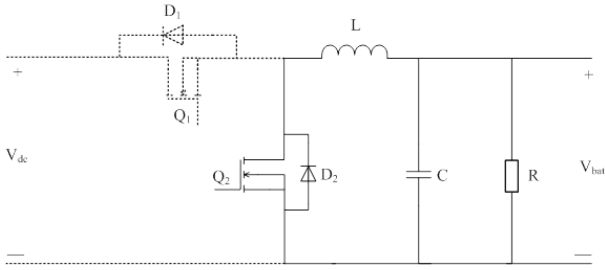


Figure 3: Equivalent circuit state of Buck mode 2

switch-off state, then the current is interrupted. The situation between the two cases is the critical current, i.e., the current in the inductor is zero at the end of the switch-off. In the bidirectional DC/DC converter system, the inductor current is in continuous state. Under the condition of step-down operation, the electronic component is assumed to be an ideal device. In the single cycle of PWM, two states of the circuit are analyzed below.

In the first mode of operation, when  $Q_1$  and  $Q_2$  switch off, the input voltage  $V_{dc}$  is added to  $D_2$ , inductance, and capacitance. The inductor current increases continuously, and the electric capacitor voltage is maintained constantly [21].

The equivalent circuit state of the buck mode is shown in Fig. 2. In Equation (2),  $V_i$  ranges from 30 V to 60 V,  $V_o$  is 24 V,  $R_{eq}$  is 2.4  $\Omega$ , and inductance  $L$  is 160  $\mu\text{H}$ . When  $R_{eq}$  is the dissipative resistance, Equations (3) and (4) can be obtained from the analysis of the circuit, where  $i_L$  is the current through the inductor  $L$ ,  $V_{dc}$  is the fore-end input voltage,  $V_{bat}$  is the output voltage through buck mode,  $D$  is the duty ratio of the PWM signal that ranges from 0 to 1,  $T$  is a period when the switch tube works, and  $\Delta i_{L+}$  is the increase in the amount of current through the inductor  $L$ . The mathematical model of the buck converter is shown below.

$$\begin{cases} \left. \frac{V_o(S)}{V_i(S)} \right|_{d(S)=0} = \frac{D}{LCS^2 + \frac{L}{R_{eq}}S + 1} \\ \left. \frac{V_o(S)}{d(S)} \right|_{V_i(S)=0} = \frac{V_o}{D(LCS^2 + \frac{L}{R_{eq}}S + 1)} \end{cases} \quad (2)$$

$$L \frac{di_t}{dt} = V_{dc} - V_{bat} \quad (3)$$

$$\Delta i_{L+} = \frac{V_{dc} - V_{bat}}{L} DT \quad (4)$$

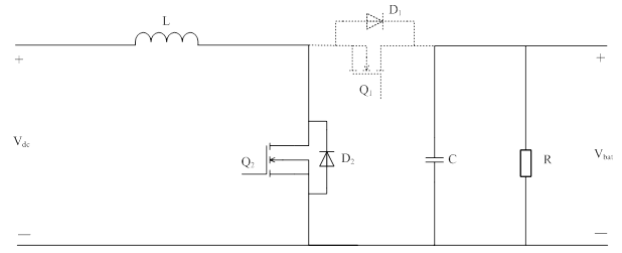


Figure 4: Equivalent circuit state of boost mode 1

In the second mode of operation, when  $Q_1$  is switched off, a loop is formed by the inductor, capacitor, and  $D_2$ , no sudden change is apparent in the current of the inductor to maintain the output voltage stability by inosculating the current of  $D_2$ , which continues to decrease the current and discharge the capacitors. The equivalent circuit in the buck mode is shown in Fig. 3 [22].

Equations (5) and (6) are analyzed in Fig. 3, in which  $\Delta i_{L+}$  is the decline variation of current through inductance  $L$ .

$$L \frac{di_L}{dt} = -V_{bat} \quad (5)$$

$$\Delta i_{L-} = -\frac{V_{bat}}{L}(1-D)T \quad (6)$$

When the circuit works in a stable state of operation, the stored current  $i_L$  occurs repeatedly in inductance, i.e., when the switch tube is switched on, the input energy of the inductor is equal to its output energy when the switch is off. This phenomenon is represented by Equation (7).

$$\Delta i_{L+} = |\Delta i_{L-}| \quad (7)$$

Equation (7) can be written to Equation (8).

$$\frac{V_{dc} - V_{bat}}{L} DT = \frac{V_{bat}}{L} (1-D)T \quad (8)$$

To sum up, the relationship between the input and output voltages of the buck circuit is shown in Equation (9).

$$V_{bat} = DV_{dc} \quad (9)$$

### 3.3. Working principle of the boost circuit

The boost structure is also divided into three states, namely, continuous, discontinuous, and critical. In the bidirectional DC/DC system, the inductor current is in continuous state. When the inductor current is continuous, the buck circuit also has two working states in one working period.

Fig. 4 shows the equivalent circuit in the first mode of operation when  $Q_2$  is switched on and  $Q_1$  is switched off. The voltage of the lithium battery is directly connected with the inductor, the inductor current continues to increase, and the storage energy also increases. The inductor current cannot be produced because  $Q_1$  is switched off, and the voltage is generated by the capacitor discharge [23].

When the DC power supply is switched off, the bidirectional DC/DC alters to boost mode, and the voltage output is

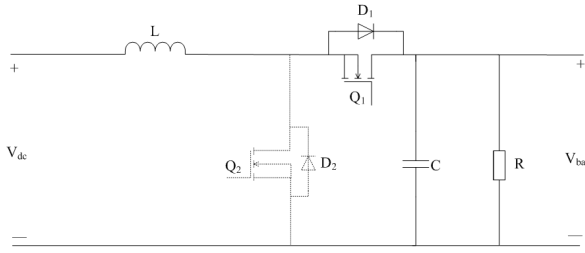


Figure 5: Equivalent circuit state of boost mode 2

stable. The duty ratio of  $Q_1$  is  $D$ , and Equation (10) is expressed as the mathematical model of the boost converter. Figure 4 shows the equivalent circuit of  $Q_2$  and the switch-off of  $Q_1$ . Equation (11) is obtained according to the circuit analysis.

$$\begin{cases} \left. \frac{V_o(S)}{V_i(S)} \right|_{d(S)=0} = \frac{D}{LCS^2 + \frac{L}{R}S + D^2} \\ \left. \frac{V_o(S)}{d(S)} \right|_{V_i(S)=0} = \frac{V_o(D^2 - \frac{L}{R}S)}{D(LCS^2 + \frac{L}{R_{eq}}S + D^2)} \end{cases} \quad (10)$$

$$V_{bat} = L \frac{di_L}{dt} \quad (11)$$

The increment of inductance current can be obtained as:

$$\Delta i_{L+} = \frac{V_{bat}}{L} DT \quad (12)$$

In the second mode of operation, when  $Q_2$  is switched off, the lithium battery and the inductive current are discharged through the diode. Given that the inductor current is inertial, the current is produced together with the supply current, and the capacitor is charged. The output voltage is stable, and the polarity remains unchanged. The inductance current decreases linearly.

Fig. 5 shows the equivalent circuit of the boost mode when  $Q_2$  works in the switch-off state, and Equation (13) is derived from the circuit analysis.

$$L \frac{di}{dt} = V_{bat} - V_{dc} \quad (13)$$

When  $Q_2$  switches off, energy is released by inductance as shown in Equation (14) below.

$$\Delta i_{L+} = \frac{V_{bat} - V_{dc}}{L} (1 - D)T \quad (14)$$

When the boost circuit is stable, the energy of changes in the inductance (when  $Q_2$  is switched on) is equal to the energy of release of inductance (when  $Q_1$  is switched off), and Equation (15) is obtained as follow.

$$\Delta i_{L+} = |\Delta i_{L-}| \quad (15)$$

Equation (15) can be rewritten to Equation (16).

$$\frac{V_{bat}}{L} DT = \frac{V_{bat} - V_{dc}}{L} (1 - D)T \quad (16)$$

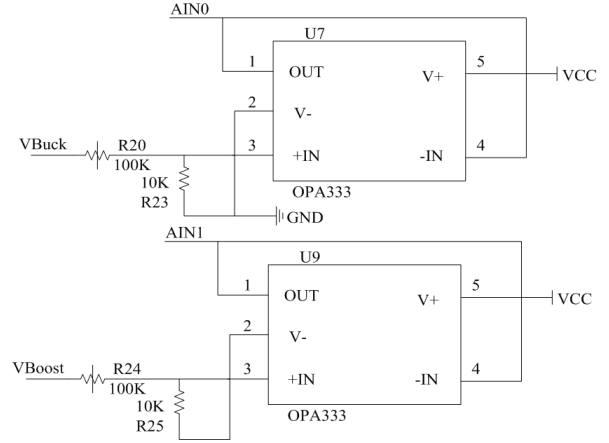


Figure 6: Voltage acquisition circuit

To sum up, Equation (17) shows the relationship between input and output voltages of the boost circuit.

$$V_{dc} = \frac{V_{bat}}{1 - D} \quad (17)$$

### 3.4. Voltage sampling principle circuit

The maximum voltage of the analog-digital converter cannot exceed the power supply voltage, i.e., the maximum voltage is less than 5 V. The output and input voltages of the bidirectional DC/DC are greater than 5 V; hence, the voltage signal is sent into the analog-to-digital converter. The signal must be adjusted for it to be within the voltage acquisition range of the analog-to-digital converter. The system adopts the method of voltage divider resistance to collect voltage signals using two resistances with high precision and low temperature to partial pressure. As the voltage signal passes through two large resistors, the driving capability of the output signal weakens, affecting the sampling accuracy of the analog-digital converter. Therefore, the voltage follower is used to perform impedance transformation to improve the output impedance, and OPA333 is chosen in the system. The voltage acquisition circuit is shown in Fig. 6.

### 3.5. Principle of current sampling

The system adopts loop series copper wire to perform current sampling. As the temperature changes, the resistance values slightly change, and copper-nickel has a low temperature coefficient of resistance. The monitor IN282 is set in the sampling process of the present study. The constantan wire is accessed between +IN and -IN, and the decline in current occurs in the constantan wire. Minor pressure difference is displayed by amplifying the chip differential amplifier 50 times. The diagram of the current sampling is shown in Fig. 7.

### 3.6. Analysis of the control system and control method

#### 3.6.1. Analysis of the control system

In the DC micro grid energy storage system, the bidirectional DC/DC converter system is mainly composed of

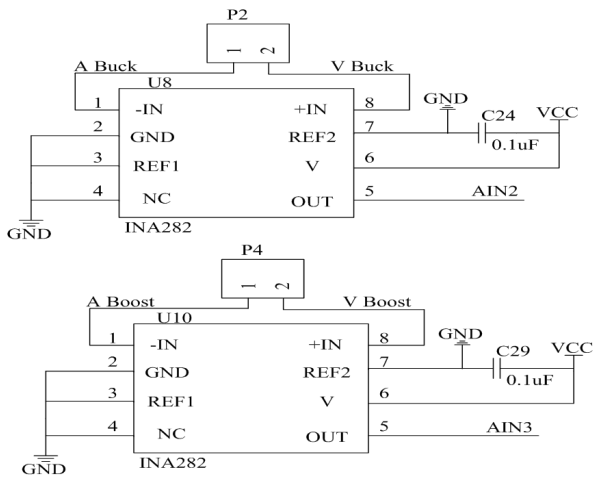


Figure 7: Current sampling circuit

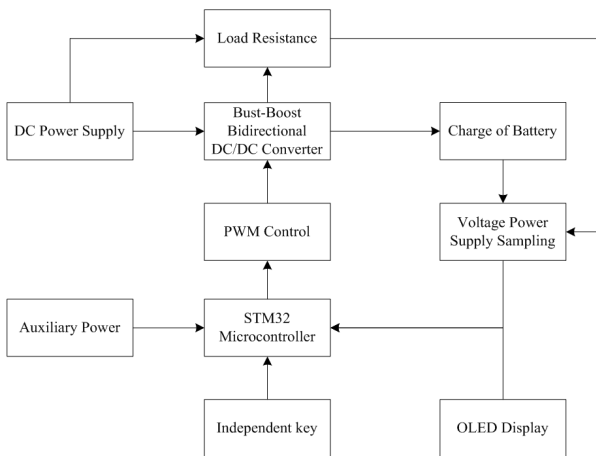


Figure 8: Component diagram of the system

a bidirectional DC/DC converter, STM32F103RBT6 microcontroller, A/D analog acquisition, voltage sampling circuit, current sampling circuit, switching circuit, auxiliary power supply circuit, and protection circuit module. The topology of the converter is a buck-boost type, and the main circuit is bidirectional half bridge. When the DC regulated power supply is connected, the power is supplied to the bidirectional DC/DC converter and the load resistor, and the converter output voltage is charged to the battery pack. The voltage and current of the load resistance and the voltage of the battery pack are sent back to the microcontroller by the sampling circuit, and the duty cycle of the PWM wave is changed by PID operation to adjust the voltage and current in real time. When the power supply is switched off, the battery pack is boosted by a bidirectional DC/DC converter and output to the load resistor. The auxiliary power [24] is supplied to the control system, which can switch the working mode or adjust the voltage and current parameters using the independent key. The working parameters of the converter can be displayed in real time by OLED (Organic Light-Emitting Diode). The flow chart of the system is shown in Fig. 8, and

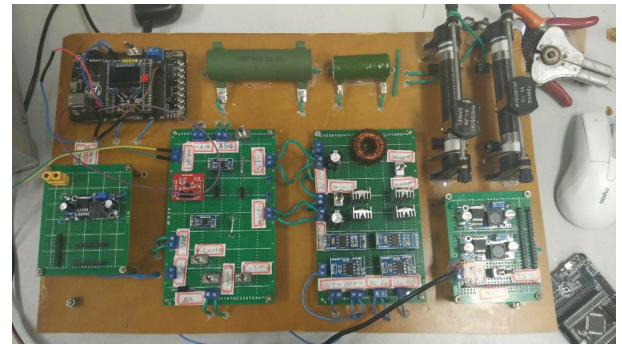


Figure 9: Physical diagram of the system

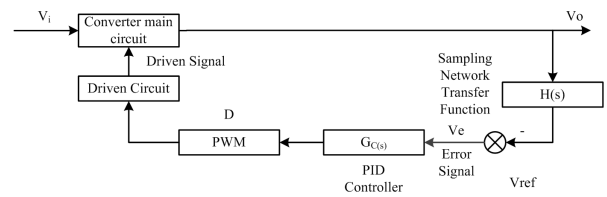


Figure 10: Structural diagram of constant voltage control

the physical diagram of the system is shown in Fig. 9.

### 3.6.2. Closed-loop PID control mode with constant voltage

Constant voltage control is mainly used for constant voltage charging and output of the lithium battery. The voltage signal is sampled by a resistor divider and AD converter and is then fed back to the STM32 microcontroller. The duty ratio is adjusted by PID operation to form a closed-loop voltage negative feedback control system. The constant pressure control structure diagram is shown in Fig. 10 [25].

### 3.6.3. Closed-loop PID control mode with constant current

Constant current control is mainly used in the constant current charging phase of lithium batteries. Similarly to constant voltage control, the current is collected by the constantan wire, the system adopts the INA282 to be in the I/V transform process, and the current is amplified by the AD converter to feed back to the STM32 microcontroller. Given that the system uses the PID algorithm to adjust the duty ratio of PWM wave and the output current, a current closed-loop negative feedback control system can be composed. A structural diagram of constant current control is shown in Fig. 11.

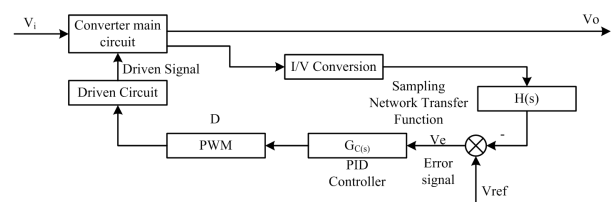


Figure 11: Structural diagram of constant current control

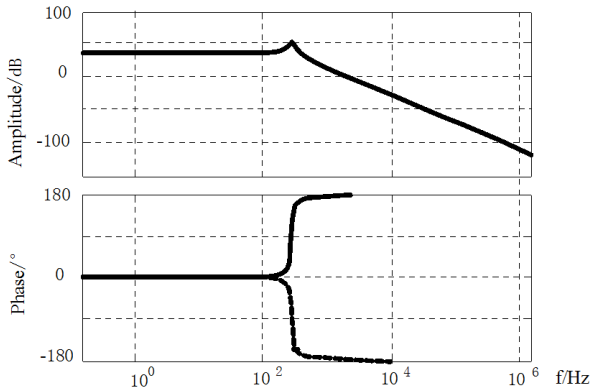


Figure 12: Bode diagram without compensation in buck model

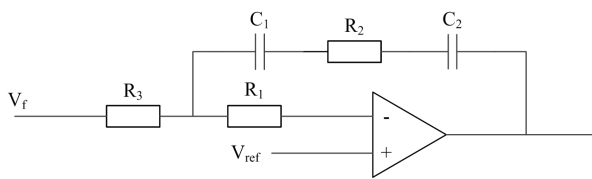


Figure 13: Analog PID voltage compensation circuit

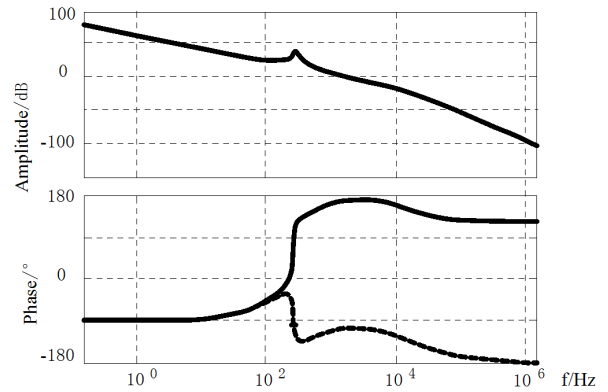


Figure 14: Bode diagram with compensation in buck model

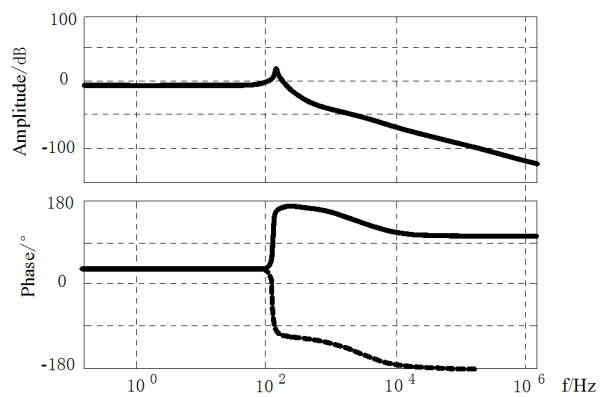


Figure 15: Bode diagram without compensation link in boost mode

## 4. Result analysis and discussion

### 4.1. Influence of PID voltage compensation on the system stability of buck mode

In the absence of compensation action, by controlling the expression to the output, the buck mode bode diagram without compensation is shown in Fig. 12. When the output is reduced, the opened-loop transfer function of the system produces two poles of the right plane without the compensation mode, and the corresponding bode diagram is represented by the solid part of Fig. 12. The amplitude–frequency characteristic curve is the same in the two cases, but the phase frequency curve is symmetrical with a zero-degree line [26].

For the common buck topology, the use of P, PI, and PID control methods can enable the system to achieve better stability. However, when the main circuit exists with a negative impedance load, two poles exist in the Q's right side; its phase frequency curve and resonant frequency reach approximately 180 degrees through the proportional regulator or proportional integral regulator, which cannot make closed-loop control system work in a stable state.

According to the Nyquist criterion, if the system passes through  $\pi/2$  once, then the system with 2 S's right poles can be stabilized. The differential mode can generate the phase compensation with  $\pi/4$ , so the PID control methods can make the buck mode of the bidirectional DC/DC converter function in a closed-loop stable state. The traditional analog PID compensation circuit is shown in Fig. 13.

This study can generate Fig. 14, which is a bode diagram of the compensation link in buck mode, by setting the appropriate parameters of the PID compensation link. The dissipative load is represented by the dotted line, and the source

load is represented by the solid part. When the opened-loop switch-off frequency is 1.28 kHz, in which the phase margins are 64 degrees and 51 degrees [27] under the state of the source load, the system can achieve better stability.

### 4.2. Influence of boost mode on system transformation stability

As shown in Fig. 15, the bidirectional DC converter operates in boost mode and controls the output bode diagram. The bode diagram is in boost mode without compensation link. The system has a zero-right half plane. The dotted line represents the system existing in the dissipative class load, and the solid line represents the system existing in the source-type load. In Fig. 16, the system exists in differential mode, which can enable the system to function in a stable working environment. Therefore, the analog PID controller can also be shown in Fig. 16 to generate the bode diagram with PID compensation link. After the system is compensated, the system works in a stable working environment [28].

Table 1: Test of constant current charging and current display with  $U_2 = 30$  V

Current Value, A	Actual value, A	Display value, A	Current-controlled accuracy, %	Current measurement accuracy, %
1	1.026	1.014	2.6	1.17
1.2	1.205	1.199	0.42	0.5
1.4	1.439	1.427	2.79	0.83
1.6	1.587	1.578	0.81	0.57
1.8	1.8	1.798	0	0.11
2	2.002	1.994	0.1	0.4

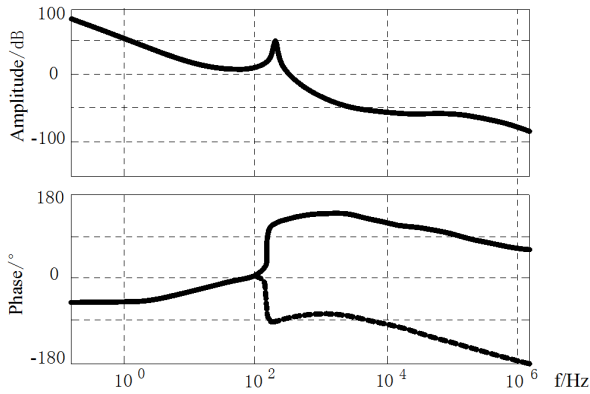


Figure 16: Bode diagram with compensation link in boost mode

Table 2: Charge current change rate and efficiency tests

Input voltage $U_2$ , V	Charging current $I_1$ , A	Current reducing rate $S_{I_1}$ , %
36	2.021	
30	2.029	0.099
24	2.023	

#### 4.3. Experiment of bidirectional DC/DC converter at constant current and constant voltage

##### 4.3.1. Constant current charging test of bidirectional DC/DC converter in charging mode

In the model of bidirectional DC/DC converter topology, the DC voltage output is adjusted so that  $U_2 = 30$  V. The detection  $I_1$  of the ammeter by series connection is expressed in the unit of battery charging. This study uses a keyboard to adjust the current from 1 A to 2 A step by step, and the step value is 0.05 A. The actual current value and current value display are recorded. For convenience of testing, the current step value is 0.2 A, and the measurement data are shown in Table 1.

##### 4.3.2. Tests of charging current change rate and efficiency for bidirectional DC/DC converter in charging mode

When the DC micro grid system works in charging mode, the influence of bidirectional DC/DC topology on the change rate and efficiency of the charging current are studied. In

Table 3: Constant voltage output and efficiency tests

Parameter	Value
Input Voltage $U_1$ , V	17.978
Output Voltage $U_2$ , V	30.000
Input Current $I_1$ , A	1.836
Output Current $I_2$ , A	1.056
Efficiency of boost converter $\eta_2$ , %	95.970

Table 4: Constant voltage output measurement under automatic switching statement

DC power supply output voltage $U_S$ , V	Output voltage $U_2$ , V
32	29.92
33	29.92
34	30.06
35	30.09
36	30.09
37	30.01
38	30.06

this experiment, the charging current is set to 2 A, and the DC voltage regulator is adjusted between 24 V and 36 V. The measurement data are shown in Table 2. The current change rate  $S_{I_1}$  is calculated by  $S_{I_1} = |(I_1 - I_2)/I_1| \cdot 100\%$ .

##### 4.3.3. Constant voltage output and efficiency tests of bidirectional DC/DC converter in discharge mode

When the DC micro grid system works in discharge mode, the actual data of bidirectional DC/DC converter conversion efficiency in constant voltage output mode are obtained through the experimental test. In the experiment,  $U_2$  is kept at  $(30 \pm 0.5)$  V; the input current, input voltage, and output current are measured. The measurement data are shown in Table 3, and in this Table 3, and the efficiency of the converter is calculated by  $\eta_2 = \left| \frac{U_2 I_2}{U_1 I_1} \right| \cdot 100\%$ .

##### 4.3.4. Constant voltage output measurement of bidirectional DC/DC converter in automatic switching mode

The output voltage  $U_2$  changes as experiments are conducted to explore how the DC micro grid system can be



made to function in system switching mode. In this experiment, the system works in automatic switching mode to adjust  $U_S$  between 32 V and 38 V, and the output voltage  $U_2$  is measured. The measurement data are shown in Table 4.

## 5. Conclusions

The buck-boost topology model of the bidirectional DC/DC converter was established to increase the stability of busbar voltage in the DC micro grid system. Numerical simulation and experimental study were used to integrate the energy of the DC micro grid system. The hardware circuit of the bidirectional DC/DC converter in the system, the characteristics of the efficiency of the converter in charging mode, and the constant voltage output were studied and analyzed. The following conclusions were drawn:

1. The DC micro grid energy storage system can work in both charging mode and discharge mode and can be switched automatically according to requirements.
2. When the DC micro grid energy storage system works in charging mode, the accuracy of current control is greater than 5%, the charge current rate of change is less than 1%, and work efficiency is greater than 90%. When the charging voltage reaches the busbar voltage, the system can switch off the state of charging.
3. When the DC micro grid energy storage system works in discharge mode, the efficiency of the converter is greater than 95%. When the supply voltage of the system is changed, the energy storage system can switch the working mode automatically to maintain the stability of output voltage  $U_2$  at  $30 \pm 0.5$  V.

This study proposes a control method that applies closed-loop PID technology based on the bidirectional DC/DC converter in the DC micro grid energy storage system to improve the stability of busbar voltage when the DC micro grid energy transforms in bidirectional directions, which can form the subject of future study on the stability of micro grid voltage. However, in the future study, an advanced control algorithm must be combined with the model and modified by further optimization of the software and hardware design to control the stability of the busbar voltage more accurately when the system is in a state of energy transformation in bidirectional directions.

## References

- [1] Q. Zhong, Y. Yi, Analysis and simulation of voltage drop problem in power users, *Journal of Electric Power Systems and Automation* 20 (6) (2008) 102–106.
- [2] R. Shao, J. Han, Zhengwei nad Lin, Power quality index analysis, *Journal of Power System and Its Automation* 19 (3) (2007) 118–121.
- [3] Y. Liu, C. Huang, L. Ou, et al., Three-phase unbalanced voltage sag detection method based on dq transform, *Journal of Power System and Automation* 19 (3) (2007) 72–76.
- [4] Y. Zhou, W. Luo, Design and simulation of bidirectional DC/DC converter topology, *Automation Expo* 10 (2012) 102–105.
- [5] X. Liang, Simulation and design of dc/dc converter control, Ph.D. thesis, Qingdao University of Science and Technology, Qingdao (2016).
- [6] D. M. Xu, X. Wu, J. Zhang, Z. Qian, High power high frequency half-wave-mode ZCT-PWM full bridge DC/DC converter, in: *Applied Power Electronics Conference and Exposition, 2000. APEC 2000. Fifteenth Annual IEEE*, Vol. 1, IEEE, 2000, pp. 99–103.
- [7] K. Ramya, V. Jegathesan, Comparison of pi and pid controlled bidirectional dc-dc converter systems, *International Journal of Power Electronics and Drive Systems* 7 (1) (2016) 56.
- [8] N. Jabbour, C. Mademlis, I. Kioskeridis, Improved performance in a supercapacitor-based energy storage control system with bidirectional dc-dc converter for elevator motor drives, in: *International Conference on Power Electronics, Machines and Drives (PEMD'14)*, IET, Manchester, UK, 2014.
- [9] G. Borocci, F. G. Capponi, G. De Donato, F. Caricchi, Closed-loop flux-weakening control of hybrid-excitation synchronous machine drives, *IEEE Transactions on Industry Applications* 53 (2) (2017) 1116–1126.
- [10] Z. Yu, L. Nie, H. Lv, et al., A review of DC access technology for electric vehicle charging station, *Journal of Electrical and Mechanical Engineering* 32 (2) (2015) 279–284.
- [11] D. Jiang, F. Liu, R. Mao, X. Yuan, Buck-boost integrated three-port DC-DC converter with coupling inductor, *Automation of Electric Power System* 38 (3) (2014) 7–13.
- [12] Y. Cai, C. Wang, Y. Wang, Study on dab lcc resonant bidirectional dc/dc converter, *Journal of Coal Engineering* 47 (2) (2015) 92–94.
- [13] P. Lin, Bidirectional DC/DC converter designing based on microcomputer, *Computer Knowledge and Technology* 13 (13) (2017) 210–211.
- [14] X. Wei, D. Dai, New type bi-directional DC/DC converter PID control based on arranging transient process, *Journal of Electric Power Science and Engineering* 33 (8) (2017) 6–12.
- [15] L. Zhao, J. Li, W. Fan, Y. Zhang, X. Zhang, Design of bidirectional DC/DC converter based on STC89C51, *Journal of Electrical Design* 5A (2017) 56–57.
- [16] F. Z. Peng, H. Li, G.-J. Su, J. S. Lawler, A new ZVS bidirectional DC-DC converter for fuel cell and battery application, *IEEE Transactions on power electronics* 19 (1) (2004) 54–65.
- [17] C. Shi, X. Tang, N. Li, G. Sun, Y. Sun, Dc conversion technology based on full bridge isolation bidirectional converter, *Journal of Electrotechnical Society* 31 (2) (2016) 121–127.
- [18] Y. Tong, G. Wu, X. Jin, et al., Topological study of bidirectional dc/dc converters, *Proceeding of the CSEE* 27 (13) (2017) 81–86.
- [19] F. Akar, Y. Tavasoglu, E. Ugur, B. Vural, I. Aksoy, A bidirectional non-isolated multi-input DC–DC converter for hybrid energy storage systems in electric vehicles, *IEEE Transactions on Vehicular Technology* 65 (10) (2016) 7944–7955.
- [20] G. Waltrich, M. A. Hendrix, J. L. Duarte, Three-phase bidirectional dc/dc converter with six inverter legs in parallel for ev applications, *IEEE Transactions on Industrial Electronics* 63 (3) (2016) 1372–1384.
- [21] K. Lang, W. Lin, Y. Xu, Current status of two-way dc/dc converter circuit topology, in: *China Electrotechnical Society of Electric Power Society Academic Conference, China, Beijing, 2008*, pp. 1–5.
- [22] Y. Zhang, Y. Gao, J. Li, M. Sumner, Interleaved switched-capacitor bidirectional DC-DC converter with wide voltage-gain range for energy storage systems, *IEEE Transactions on Power Electronics* 99 (2017) 1–16.
- [23] L. Huang, X. Dong, C. Xie, S. Quan, Y. Gao, Research and modeling of the bidirectional half-bridge current-doubler DC/DC converter, *International Journal of Rotating Machinery* 2017.
- [24] R. Anand, P. M. Mary, Improved dynamic response of dc to dc converter using hybrid pso tuned fuzzy sliding mode controller, *Circuits and Systems* 7 (06) (2016) 946–955.
- [25] R. S. Balog, P. T. Krein, Bus selection in multibus dc microgrids, *IEEE Transactions on Power Electronics* 26 (3) (2011) 860–867.
- [26] G. Lu, L. Zhang, Y. Bu, Y. Zhou, Study on front-end bidirectional dc/dc converter of photovoltaic grid-connected inverter, *International Journal of Mechatronics and Applied Mechanics* 1 (2017) 45–52.
- [27] F. Zhang, Two-way DC/DC converter, Master's thesis, Nanjing University of Aeronautics and Astronautics, Nanjing (2005).
- [28] F. Zhang, C. Zhu, Y. Yan, Control model of bidirectional DC/DC converter, *Proceeding of the CSEE* 25 (11) (2015) 46–49.